Curvature strains as a global orchestrator of morphogenesis

Julius B. Kirkegaard⬤
Niels Bohr Institute, University of Copenhagen, 2100 Copenhagen, Denmark

Successful morphogenesis on the scale of organs or organisms requires strict coordination between the constituent cells whose action on the local scale must be orchestrated accurately to achieve a functional shape on the global scale. We present a theoretical model in which morphogenetic information is encoded only through a locally preferred curvature, but with cell dynamics which simultaneously ensures that these interactions globally achieve morphogenesis and correct cell-neighbor exchanges to avoid cell stretches. This is achieved by a cell-cell interaction potential that drives correct cell intercalation to reorganize the cell sheet dynamically during the deformation processes. We demonstrate morphogenesis of simple three-dimensional shapes and study the effects of fixed cell neighbor connectivity and noisy cell division.

I. INTRODUCTION

The development of an embryo represents perhaps the greatest spectacle in the biological realm of Nature. The result of millions of years of evolution plays out on the time scale of days, displaying a complexity that easily overshadows any manmade creation. As an embryo grows, each constituent cell must "decide" its migratory path in such a way that the organism as a whole reaches its desired functional shape. This decision process is complicated by the fact that cells constantly divide, interchange neighbors, differentiate, deform, and undergo apoptosis.

The study of cell migration in morphogenesis can be divided into two main aspects: what cell-cell interactions allow for the correct morphology and cell neighbor topology to be achieved locally? And how are these processes coordinated on a global scale? For instance, in embryos of *Drosophila melanogaster* [1,2], early global information is provided locally in terms of the pair-rule genes that segment the body plan of the fruit fly [3]. The expression of these genes is determined by a gene regulatory network influenced by the gap genes, which in turn are regulated by maternal genes controlled by the mother fly [4–9]. These hierarchical layers of gene regulatory networks provide global information at the local scale, which is subsequently used to guide cell differentiation, migration, and deformation. The signals, in fact, need not be chemical as physical forces have also been shown to influence morphogenesis [10].

Studies of morphogenesis typically focus on understanding important morphogenetic processes or stages in isolation with examples including buckling [11–14], neurulation [15–18],

gastrulation [19–21], tip growth [22–24], and inversion [25–27]. To understand the underlying mechanisms driving these processes, several distinct theoretical tools have been developed [28], but it remains a challenge to find a single, general model that unveils intrinsic properties of vastly different processes and stages. Cellular Potts models have been adapted to model morphogenesis by having collections of lattice points represent cells [29–31]. In contrast, discrete cellular models represent cells directly: By modeling the dynamics of border points between cells, vertex models can describe the dynamics of a finite collection of cells [32]. These models are typically used to study two-dimensional phenomena [33–35], but have seen applications in three dimensions as well [36–39]. Centroid models prescribe instead the dynamics of cell centers and model interactions between cells with effective potentials [40–43], and can typically model larger systems compared to vertex models. Finally, collections of cells may be approximated as a continuum of active material to study large-scale morphogenesis such as in active gel physics [44] or to directly relate biological cell sheets with their inanimate counterparts known from condensed and soft matter physics [45,46]. These approaches range from full-scale finite element simulations [17,18,47] to models of thin elastic sheets [25–27,48–56], which have the distinct advantage that much of their dynamics can be understood analytically.

As these theoretical models each come with distinct advantages, they are typically used to study specific processes in isolation. For instance, proteins are known to induce intrinsic curvature strains [49], which in continuum elastic sheet models can explain the dynamics of complex deformation processes [25,26,55,57]. Yet, the drawback of this approach is that individual cells are not modeled, and thus effects of, e.g., cell neighbor rearrangement can only be approximated in certain systems [58,59]. But cell rearrangement (intercalation) is a critical component in many morphogenetic systems with large-scale deformations as it allows for natural relaxation of the cell sheet and the elongation of shapes by reorganizing of
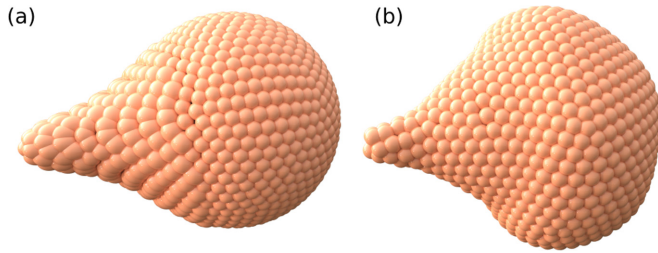

(a) (b)

FIG. 1. Pulling on a sphere. (a) Stretches emerge when there is no cell rearrangement and thus individual cells must grow or be stretched to ensure a confluent sheet. (b) With cell neighbor rearrangement the distance between cells (or, equivalently, the size of cells) can be kept constant under shape deformations. The cell sheets in (a) and (b) have the same number of cells.

cells as opposed to stretching (Fig. 1) as exemplified by the process of convergent extension [31,42,60–64].

In this paper, we present a *discrete* cell model that is directly linked to the theory of elastic sheets driven by curvature strains. The model allows us to study large deformations of cell sheets while naturally maintaining intercellular distances and cell sizes through cell rearrangements. We thus show that intrinsic curvature strains cannot only drive shape deformations, but also directly drive cell rearrangements to avoid cell sheet stretches.

While a bottom-up approach is often taken in the study of morphogenesis, where careful tuning of model parameters are done to examine a specific shape deformation [16,25,36], we instead demonstrate the generality of our model with a top-down approach [66–68]. Thus we derive parameters directly from desired final shapes and simulate the emergence of such predefined shapes from a single cell-cell interaction potential. We demonstrate that our model can be used to deform a cell sheet into desired complex shapes while maintaining constant cell sizes. While we do not model the signaling directly, we show that signals exist that transform continuously two shapes into one another via local interactions only. Thus this work ties into recent work on cellular automata demonstrating that simple neural interaction rules can lead to desired two-dimensional morphogenetic profiles [68].

II. MODEL

We consider a collection of cells that form a thin sheet and take a top-down approach with the goal to define an interaction potential V between cells, the dynamics of which leads to desired shapes. Mathematically, we can express our desire in the definition of V as

$$\{\boldsymbol{x}_i\}_{\text{final shape}} = \arg\min V(\{\boldsymbol{x}_i\}), \tag{1}$$

where $\boldsymbol{x}_i$ is the location of cell i. Dynamically, such a minimum is reached from overdamped dynamics of the form

$$\partial_t \boldsymbol{x}_i = -\nu_i \frac{\partial V}{\partial \boldsymbol{x}_i}. \tag{2}$$

If the minimum is unique, the values of the mobilities ν_i do not matter for the final shape found; and in fact, we can choose these to optimize the speed of our simulation [69]. We define

our potential as a sum of potentials from each cell,

$$V = \sum_i V_i, \tag{3}$$

where V_i, defined below, is the result of interactions between cell i and the rest of the cells.

We will refrain from introducing a discontinuous concept of neighboring cells as this approach typically results in discontinuous jumps in the potential on cell rearrangements [38,42]. Instead, we define interaction potentials that decay quickly with distance between cells. Concretely we distribute the interaction of cell i to the other cells according to the matrix

$$w_{ij} = \frac{e^{-\|\boldsymbol{x}_i - \boldsymbol{x}_j\|^2 / l}}{\sum_j e^{-\|\boldsymbol{x}_i - \boldsymbol{x}_j\|^2 / l}}, \tag{4}$$

where the index j refers to another cell in the simulation and l is a characteristic distance. The more cells that surround cell i, the smaller each interaction becomes, emulating the fact that cells with many neighbors will share less surface area with each individual cell. This rescaling is physical when we assume that the cells form a closed surface, but the model, nonetheless, also works without the normalization. Note that the cell-cell interaction could be chemical rather than physical, but even in the case of diffusing molecules that drive the interactions may these be described by a neighbor interaction function.

Our potential is then divided into three terms

$$V_i = \alpha_c V^i_{\text{curvature}} + \alpha_d V^i_{\text{distance}} + \alpha_s V^i_{\text{sheet}}, \tag{5}$$

where the α's are constants. The first term, $V_{\text{curvature}}$, is inspired by the theory of continuum cell sheets in which curvature strains drive shape changes. All shape information will be encoded as intrinsic curvature in this term. Importantly, we are modeling individual cells and thus we need to ensure that their sizes remain constant to ensure that the sheet is neither stretched nor compressed locally. This is achieved indirectly by ensuring that cells stay at a preferred distance from one another. We impose this as a soft constraint with the second term V_{distance}. It is the interplay between these two terms that is crucial to the dynamics of the model: the former controls shape and the latter ensures correct cell rearrangement. The last term, V_{sheet}, emulates the interactions with cells inside the sheet and is needed to ensure the stability of a sheet of individual cells.

The distance potential keeps cell sizes relatively constant by imposing short-ranged repulsion due to steric interactions and attraction at longer ranges. At long distances, we impose Hookean elasticity with a preferred intercell distance of ℓ:

$$V^i_{\text{distance}} = \sum_j w_{ij} \frac{(\|\boldsymbol{x}_i - \boldsymbol{x}_j\| - \ell)^2}{\|\boldsymbol{x}_i - \boldsymbol{x}_j\|^{1/3}}. \tag{6}$$

The denominator ensures hard-core repulsion at small distances. The sum runs over all other cells j, weighted by their interaction strength w_{ij}.

In the following, we derive a discrete version of the second fundamental form $\mathbf{c}_i$ known from continuum theories. The curvature potential is then simply defined as a curvature
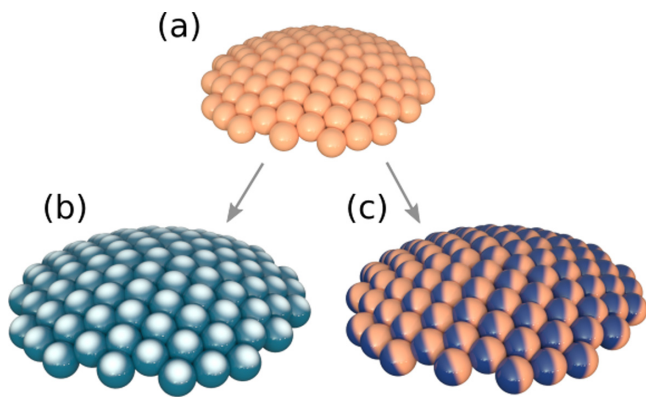
FIG. 2. Cell polarity. On a cell sheet (a), the apical-basal polarity (b) distinguishes one side of the sheet from the other. In contrast, a planar polarity (c) sets a local direction within the sheet. The direction of polarity is indicated by a color gradient, which in turn could be interpreted as the asymmetrical distribution of molecules inside each cell [65].

strain between the local fundamental form and its intrinsically desired value $\mathbf{c}_i^0$,

$$V_{\text{curvature}}^i = \left|\left| \boldsymbol{c}_i - \boldsymbol{c}_i^0 \right|\right|^2. \tag{7}$$

This is similar to a Helfrich curvature term [48] except that we allow coordinate-dependent terms for reasons to be explained in a moment. The intrinsic value $\mathbf{c}_i^0$ may be derived from a desired shape. The time scales of adjusting to a preferred curvature are much slower [minutes – hours] than that of maintaining a preferred distance to adjacent cells [seconds]. This is reflected in the fact we will require $\alpha_c \ll \alpha_d$.

To define $\mathbf{c}_i$ we endow each cell with polarities [42,61,70,71], which amounts to assigning unit vectors to all cells. Biologically, apical-basal (AB) polarity is responsible for distinguishing the inside from the outside of a cell membrane [Fig. 2(b)]. This polarity evolves dynamically by interacting with the relative position of the cells [42,43]. In the present formulation, we consider the polarity fully annealed and choose AB polarity $\boldsymbol{p}_i$ to always be orthogonal to the local tangent plane of the cell sheet, which may mathematically be calculated using singular value decomposition.

In a similar fashion, one may define a polarity $\boldsymbol{q}_i$ that lies within the planar cell sheet, i.e., orthogonal AB polarity [Fig. 2(c)]. For instance, in epithelial skin cells, such a planar cell polarity is responsible for orienting the direction in which hair combs [72], but we do not enforce any specific biological meaning to the polarity introduced here. A planar polarity is not uniquely defined from the cell positions. However, if each cell stores a scalar value q_i, we may uniquely define it as proportional to the discrete gradient of this scalar field, $\boldsymbol{q}_i \propto \sum_j w_{ij}(q_i - q_j)(\boldsymbol{x}_i - \boldsymbol{x}_j)$. This vector field will have singularities at the stationary points of the q field. Lastly, a third polarity could be formed by $\tilde{\boldsymbol{q}}_i = \boldsymbol{p}_i \times \boldsymbol{q}_i$.

Having defined polarities, we can use them in various combinations to define curvature. In fact, the polarities form a local coordinate system of the tangent plane. We will exploit this fact to formulate a discrete version of the second fundamental form, which locally describes curvature. The position of cells close to cell i can be described in a local coordinate
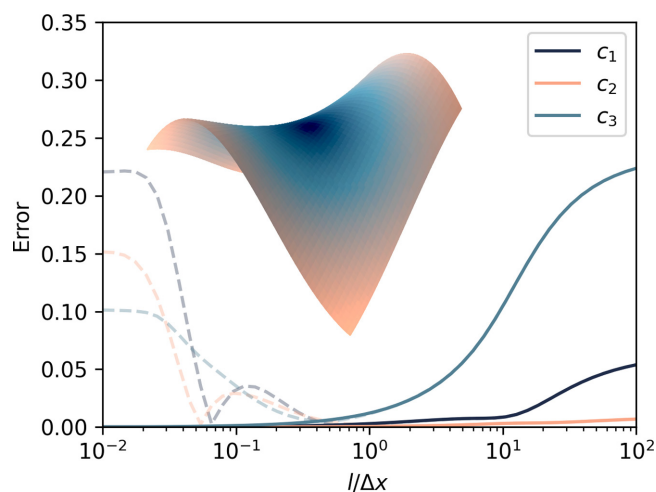

FIG. 3. Evaluating the discrete approximation to the second fundamental form on example shape given by $z = (1 + \sin(xy))\cos(x)$, which has $\boldsymbol{c} = (-1/2,\ 0,\ 1)$ at the origin. Solid lines show error on the perfect shape, which for small l behaves linearly in l. Dashed lines show error when the shape is perturbed by 1% (Gaussian) noise on all particles. Δx is interparticle distances in the xy plane. Calculated error is the absolute difference between estimated and true value of the curvature.

system as

$$\boldsymbol{x}_j = \boldsymbol{x}_i + a_{ij}\boldsymbol{q}_i + \tilde{a}_{ij}\tilde{\boldsymbol{q}}_i + b_{ij}\boldsymbol{p}_i. \tag{8}$$

In other words, one can get from $\boldsymbol{x}_j$ to $\boldsymbol{x}_i$ by moving along the unit vectors $\boldsymbol{q}_i$, $\tilde{\boldsymbol{q}}_i$ and $\boldsymbol{p}_i$ an amount a_{ij}, $\tilde{a}_{ij}$, b_{ij}, respectively.

We then define the local fundamental form $\boldsymbol{c}_i$ as the least-squares solution to second-order polynomial expansion $b_{ij} \approx c_{i1}a_{ij}^2 + c_{i2}\tilde{a}_{ij}^2 + c_{i3}a_{ij}\tilde{a}_{ij}$ describing the displacement of the cells along the AB polarity in terms of the displacement along the planar polarity directions. We define the best expansion as the one that minimizes the squared error weighted by w. Minimizing $\sum_j [w_{ij}(a_{ij}^2 c_{i1} + \tilde{a}_{ij}^2 c_{i2} + a_{ij}\tilde{a}_{ij}c_{i3} - b_{ij})]^2$ we obtain

$$\boldsymbol{c}_i = \begin{pmatrix} w_{i1}\,a_{i1}^2 & w_{i1}\,\tilde{a}_{i1}^2 & w_{i1}\,a_{i1}\tilde{a}_{i1} \\ w_{i2}\,a_{i2}^2 & w_{i2}\,\tilde{a}_{i2}^2 & w_{i2}\,a_{i2}\tilde{a}_{i2} \\ \vdots & \vdots & \vdots \\ w_{iN}\,a_{iN}^2 & w_{iN}\,\tilde{a}_{iN}^2 & w_{iN}\,a_{iN}\tilde{a}_{iN} \end{pmatrix}^{\dagger} \begin{pmatrix} w_{i1}\,b_{i1} \\ w_{i2}\,b_{i2} \\ \vdots \\ w_{iN}\,b_{iN} \end{pmatrix}, \tag{9}$$

where $\dagger$ denotes the Moore-Penrose pseudoinverse. Our method stands in contrast to how the second fundamental form is typically calculated in a discrete settings. The need for a custom approach arises because we do not enforce a neighborhood mapping on the cells as is the case for triangulated surfaces [73] or when using Voronoi-induced neighbors [42]. Figure 3 demonstrates the correctness of our approach on a sample surface. For surfaces that are not quadratic (as in the example of Fig. 3) our approach is naturally only an approximation, and one that depends on the characteristic distance l in Eq. (4). The error of the approximation is $\mathcal{O}(l)$. Nonetheless, we take l to be on the order of the finite cell-separation distance, which regularizes the calculation to be robust against noise as demonstrated by the dashed lines in Fig. 3.
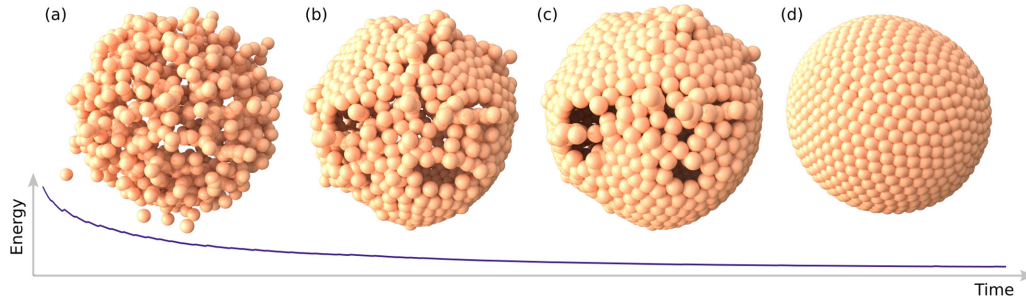
FIG. 4. Assembly of a spherical shell. Stability of the model is demonstrated by adding positional noise to a spherical shell. The disrupted shell (a) then reassembles (b),(c) to a cell sheet (d). The graph shows the decrease in potential energy during the process. *Parameters:* $\alpha_c = 0.1$, $\alpha_d = 50$, $\alpha_s = 0.5$.

Finally, we need to define the interactions that ensure the cells remain in a sheet. This is not needed if $c = c^0$. However, when the current and intrinsic curvatures are far apart, we need an extra interaction to ensure a stable sheet. Had we modeled solid objects, this would not be needed; but this would, in contrast, be computationally a much more expensive system to study. We assume that cell displacements out of the plane are kept in place by Hookean elasticity for small displacements, but regularized at larger displacements. As the AB-polarity vector p_i determines the tangent plane, this can be achieved using

$$V_{\text{sheet}}^i = \sum_j w_{ij} \frac{|(x_i - x_j) \cdot p_i|^2}{|x_i - x_j|^2}, \qquad (10)$$

where j is a sum over all other cells. We note that this term added to the potential will perturb the shape encoded by c^0. To counter this, the magnitude of this term (α_s) could be tuned towards zero as $c \to c^0$, but we ignore this complication here.

Finally, to simulate Eq. (2) we program the potential differentiably and use automatic gradient calculations to evaluate the forces from Eq. (5) directly [74–76].

III. RESULTS

A. Simple intrinsic curvature

We begin by exemplifying our model with simple intrinsic curvatures. With $c_i^0 = (\sigma, \sigma, 0)$ for all cells, the dynamics of our model is independent of the planar polarity (q_i). The energy minimum of this model is a spherical shell so long as the value of σ matches approximately with the curvature of the natural spherical shell permitted by the preferred cell-cell distances. Figure 4 demonstrates that even shapes without initial sheetlike structure will self-assemble to form a spherical shell. This demonstrates the stability of our model: when cell sheets are far from their equilibrium shape, they can self-organize towards it.

To define the in-plane polarity q, we start by initializing a scalar field $q_i = \arccos z_i$ on a unit sphere as illustrated in Fig. 5(a). This induces the polarity field shown in Fig. 5(b). We note that at the poles of the sphere, this vector field will be singular and so the polarity q_i here will be undefined. In practice, our scheme results in a random polarity at these points as shown in Fig. 5(b*). With planar polarity well-defined, we consider $c_i^0(t) = (\sigma_1, \sigma_2, 0)$. For $\sigma_1 < \sigma_2$ the intrinsic

curvature prefers high curvature along $\tilde{q}$ which stretches the sphere to a thin cylinder as shown in Fig. 5(c), thus demonstrating the process of convergent extension [42,61]. If, in contrast, we consider $\sigma_1 > \sigma_2$, high curvature will be preferred along q which results in the sphere becoming oblate, thus resembling a red blood cell [48] as shown in Fig. 5(d). The full parameter space of σ_1 and σ_2 is explored in Fig. 6. These simple cases illustrate the key features of our model: First, the potential term V_{distance} exactly ensures correct cell rearrangement during deformation as defined by $V_{\text{curvature}}$. This interplay assures that there are no cell sheet stretches or compressions for all shape deformations. Secondly, the input parameters are easily interpretable. The intrinsic curvatures simply encode the locally preferred shape and the discrete second fundamental form is approximately independent of the distances between cells as long as the curvature remains fixed.

The direction in which the sphere stretches is determined by the direction of the planar polarity q. Nonetheless, if we allow c_i^0 to be different for each cell i, the sphere can also be made prolate/oblate in any direction by suitably modulating the intrinsic curvature.

B. Morphogenesis

Due to constant cell rearrangement needed to form complex shapes, the value q_i cannot remain constant for each cell in general. Instead q_i should be considered a morphogen [77] that is internally regulated or externally controlled. In the development of *D. melanogaster* this is exemplified by, e.g., knirps and bicoid, [7,9,78], where, in particular, bicoid RNA is localized in the anterior end of the embryo by the maternal fly. Gene translation in combination with diffusion and degradation thus induces a bicoid protein gradient field across the developing embryo [4]. Inspired by this, we consider $q_i \propto D \sum_j w_{ij} q_j + z$, where D is a diffusion coefficient and instead of injecting morphogen exactly at one end, we inject it proportional to the distance from the end. This approach also directly breaks the symmetry of the spherical initial conditions, which in fully internally regulated systems would have to be broken spontaneously. Many other choices could be made, but this is perhaps the simplest that still provides stable planar polarity fields.

Having defined q_i, we demonstrate the morphogenesis of simple, predefined geometries. Given a desired embryo shape, the goal is to choose a $c_i^0(t)$ that transforms a sphere (or any
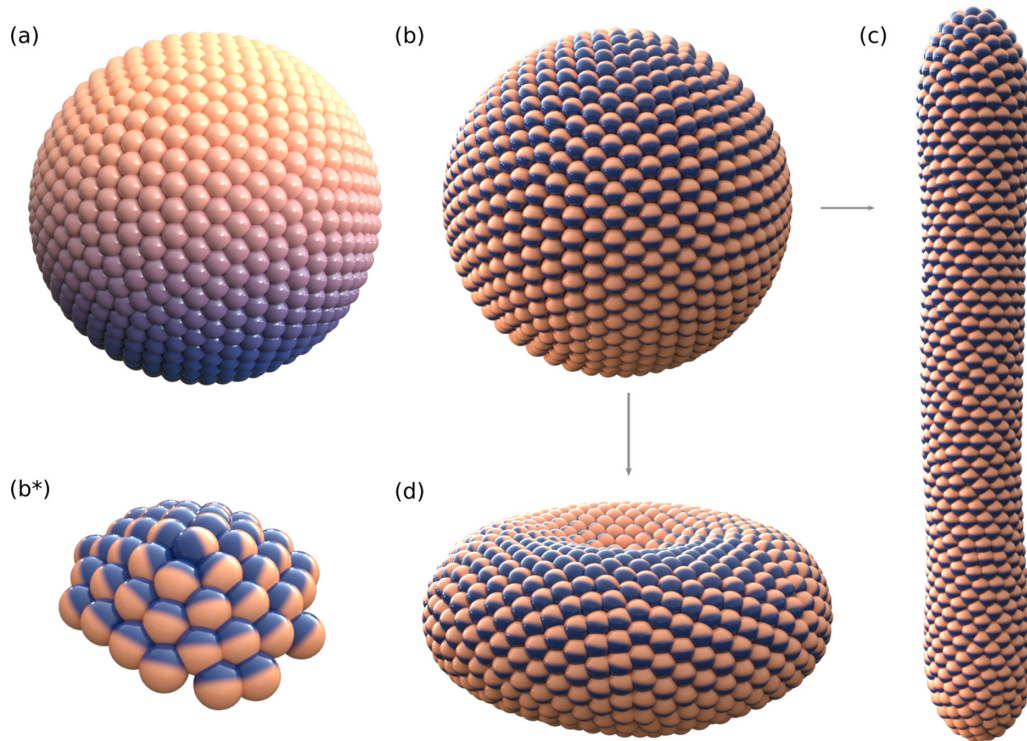
FIG. 5. Planar polarity and curvature strains. The scalar field q (a) can induce a polarity field (b) by using the local gradient. This field, however, will have at least one singularity(b*). With a well-defined planar polarity field, asymmetrical curvature strains deform the sphere in different ways. (c) $\sigma_1 < \sigma_2$ stretches the sphere to a thin cylinder. (d) $\sigma_1 > \sigma_2$ squeezes the sphere flat. These deformations further demonstrate correct cell intercalation which ensures that intercellular distances remain constant.

other initial shape) into this desired shape while constantly rearranging cells to relax the cell sheet. This "mapping" is highly noninjective, and yet very hard to design in general.

Given a shape its discrete second fundamental form may be calculated as detailed in the model section; this is the case even if the given shape does not have fixed intercell distances. In the absence of cell rearrangements, we could map the location of each cell onto the sphere and thus easily assign c_i to all cells. However, with cell rearrangements, neighbor connectivity is not preserved and we instead need to define a dynamic $c_i^0(t)$. Biologically, such dynamics would be defined by gene regulatory networks. These interactions can be approximated by, e.g., neural networks that transmit information between neighboring cells [68]. Here, we take a simpler approach: similarly to how q_i was defined above, we may define a q_i^B and q_i^C along the x and y direction, respectively. This allows us to define a function that maps from these state variables to the intrinsic curvature $c_i^0 = f(q_i, q_i^B, q_i^C)$. We choose f such that it coincides with the real curvature when evaluated on the desired shape. This could be done by, e.g., fitting a neural network or any other general function, and here we simply employ a radial basis function expansion in the space of (q_i, q_i^B, q_i^C). As elaborated in the discussion, this approach works well except at defects. A simple fix to this is to consider f the average over more than one coordinate system (using q_i, q_i^B and q_i^C).

We are now in a position where we can calculate f for any given shape. Figure 7 demonstrates the dynamics that this method leads to on two desired shapes: a "squid"-like shape with arms located at specific locations [Fig. 7(a) → 7(b)] and

a shape exhibiting the emergence of a saddle-point [Fig. 7(a) → 7(c)]. While f is only correctly defined if the cells take on the correct shape, we see that even a simple definition such as this one allows a shape which closely resembles the desired one to emerge. Most crucially, we see that cell rearrangements naturally occur and permit shape deformations similar to that seen in the process convergent extensions: with no cell stretching.

C. Fixing Neighbours & Cell Division

As we have just seen, the requirement of fixed neighbor distances during the process of morphogenesis makes it crucial that cell neighbor rearrangements are permitted. In our model, the final shape and cell neighbor arrangement is kept in place by the curvature strains defined in Eq. (7). However, if we fix w_{ij} to its value in the final shape, removing the possibility of neighbor rearrangements, we can in fact set $V_{\text{curvature}} = 0$ and still maintain a stable shape without any curvature strains or maintenance of intrinsic curvatures. This means that after the final shape has been reached, the morphology of the shape can be encoded solely by the cell neighbor connectivity. Thus the mechanism for reaching a shape and the mechanism for keeping the shape stable can be very different, and the latter can be much simpler.

The fact that a shape is stable simply due to its neighbor connectivity becomes increasingly true for bigger and bigger shapes. The more cells, the more interlocked the shape becomes if the neighbor connectivity is fixed. Local perturbations, such as cell apoptosis or division, will thus not affect
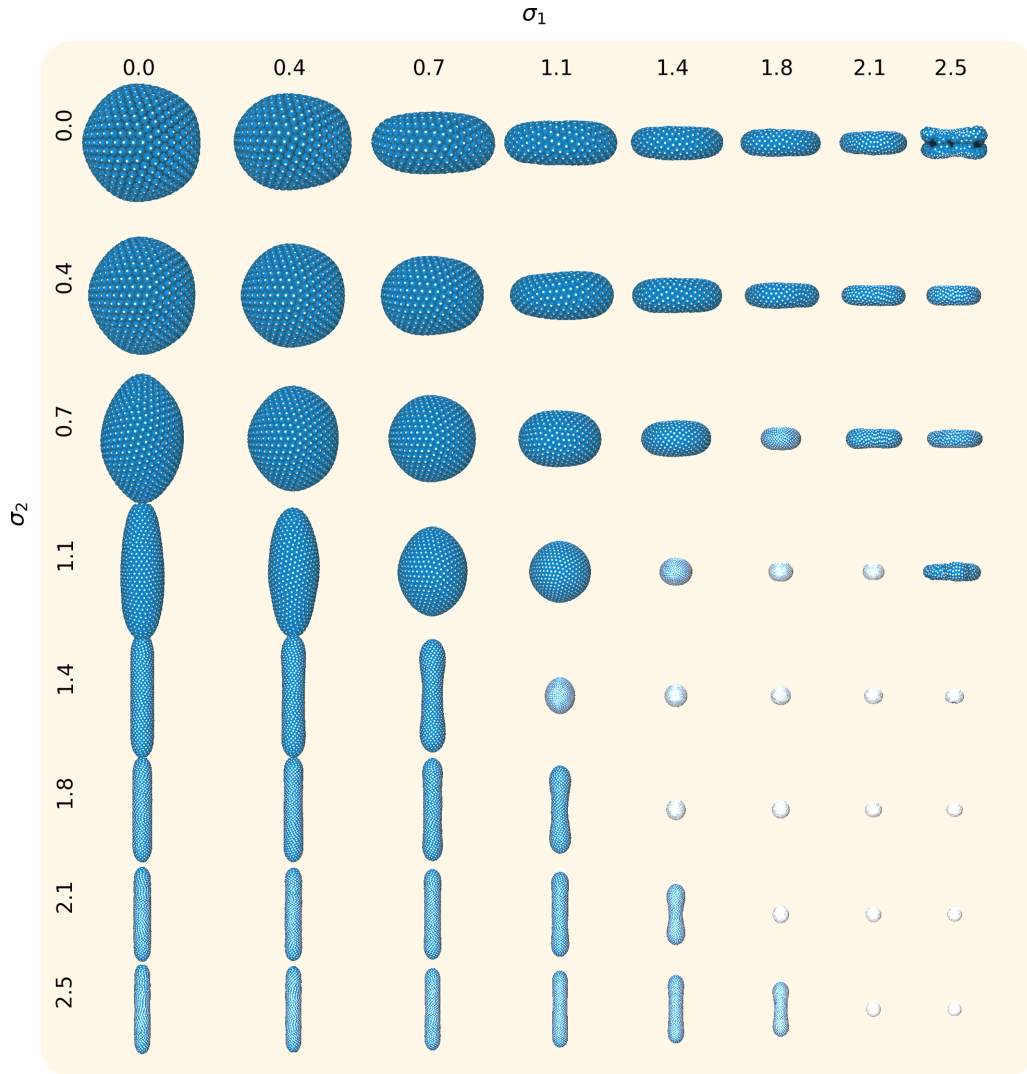
FIG. 6. Variations of σ_1 and σ_2 in $\boldsymbol{c}_i^0(t) = (\sigma_1, \sigma_2, 0)$. With $\sigma_1 = \sigma_2$, spherical shapes are obtained with varying radii depending on the preferred curvature. Off the diagonal, the shape is either squeezed flat ($\sigma_1 > \sigma_2$) or long ($\sigma_2 > \sigma_1$), with the overall size still being regulated by their absolute magnitude. For extreme values of σ, the cell sheet can break down as seen here for $\sigma_1 = 2.5$.
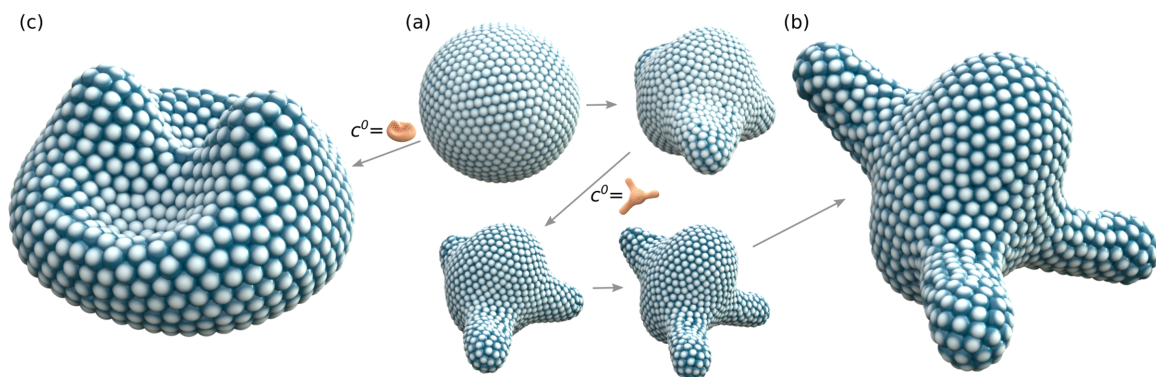

FIG. 7. Morphogenesis. (a) A sphere can be deformed to a desired shape while adhering to fixed neighbor distances by choosing c^0 correctly. (b) Example showing the deformation of a sphere to a three-armed squid. (c) Example showing deformation to a shape with a saddle point. The shapes from which c^0 have been derived need not conform to a fixed cell neighbor distance.
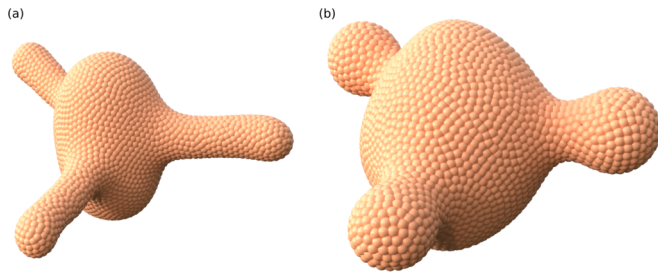
FIG. 8. Cell division from the 1500 to 3000 cells. (a) If c^0 is set to a desired shape, random cell division does not disrupt the shape [Fig. 7(b)]. (b) However, with $\alpha_c = 0$ and $\alpha_s = 1.5$, cell division changes the shape.

much global shape if this is constructed by enough cells. This is not the case for small structures, which can be perturbed by noisy events such as cell division. We implement cell division in the simplest way possible: at each time step there is a probability that a cell is divided into two with one of the daughter cells being slightly perturbed in position (in the q-$\bar{q}$ plane). The distance potential will ensure that the surrounding cells will be pushed away to make room for the new cell.

Figure 8 shows the final shape of Fig. 7(b) being subjected to cell division. We have fixed w_{ij} except during time steps of cell division, where, naturally, daughter cells must be assigned a neighbor connectivity, and the surrounding cells' neighbor weights likewise must be updated. If we keep the curvature strain potential on [Fig. 8(a)] the shape is preserved during the noisy process of cell division. However, without curvature strains [Fig. 8(b)] where the shape is maintained solely by neighbor connectivity, cell division will disrupt the overall shape as time passes. Thus neighbor connectivity cannot be responsible for keeping a shape intact during periods of large, noisy activity such as random cell division during growth. Likewise, for organisms that may regenerate limbs, such as the Axolotl, active shape regulation is needed during the regenerative process.

IV. DISCUSSION

Our main result is the demonstration that complex three-dimensional morphogenesis in a *discrete* cell model can be achieved by modulating *only* preferred curvature strains. In our formulation cell rearrangements adapts locally and are a natural consequence of the shape changes.

To achieve morphogenesis of a specific shape in our model a suitable dynamic intrinsic curvature profile $c_0(t)$ must be specified. Biologically, we can think of this as being the result of gene regulatory networks (although other drivers are also possible such as mechanical feedback). These networks could be simulated directly as well, and differentiable programming used to choose suitable network interactions similar to what has been achieved in two-dimensional cellular automata [68]. However, in the present three-dimensional case, it is more involved to define a suitable loss function. We have taken a different approach which works for the simple shapes studied in this paper. Our method emulates the result of a gene regulatory network by a simple radial basis function regressor in the space of three morphogens that diffuse across the cells. Our

approach can be interpreted as a dictionary lookup based on spatial decoding [8].

The downside of our simple approach is that we only define the preferred curvature when the cells are in the preferred shape. The complex trajectory to reach the final shape is therefore not controlled. We have demonstrated that our approach works for simple shapes, but even in these cases, there are no guarantees that the regressor does not induce shape trajectories that lead to perturbed final shapes. To generalize to more complex shapes, our method could be checkpointed, where separate regressors are used at various stages of the morphogenesis process.

Our regressor approach uses three input variables (q_i, q_i^B, q_i^C), or "coordinates", despite the fact that we are modeling a two-dimensional surface. While two coordinates locally could be sufficient, a closed surface cannot be globally described by just one coordinate system, where instead multiple charts are needed. Biologically it is indeed also the case that typically more than two morphogens are used to decode positional information [8]. Nonetheless, our current approach has the drawback that the planar polarity has at least one singularity and thus using different coordinate systems for different parts of the structure could make sense. In fact, a simple approximate solution to this is to simply have Eq. (7) be an average loss over more than one local coordinate system. Using q, q^A, q^B removes issues at the singularities.

The usual approach to define energy functionals of elastic sheets involves coordinate invariants of the second fundamental form (c). In this work, we have allowed coordinate-dependent terms in the potential due to the fact that apical-basal and planar polarity define a local coordinate system. Although the morphogen (q) used to make the planar polarity well-defined is dynamic in our model, it does not have any dynamics that relate specifically to the shape being modeled. This is why all three curvature terms (c_1, c_2, and c_3) are needed to describe arbitrary shapes. A separate approach is to have a dynamic planar polarity that orients itself along the principal curvatures. In this case, only c_1 and c_2 would be needed. While this approach is biologically more relevant, we have chosen to keep our approach as simple as possible and only use information pertaining to preferred shapes in a single term of our potential.

While cell rearrangements do have an activation cost [38,79], many discrete cell models take this to the extreme and have thermodynamically irreversible transitions. We define our model through a potential with no discontinuous jumps even during cell rearrangements. This is important to make the potential physical. Here we have defined an interaction matrix w_{ij} which, in principle, allows all cells to interact with all cells, but decreasing quickly with distance. This approach is well known from condensed matter physics, and is perhaps the simplest way to make neighbor interactions reversible. More well-known in cell models (such as vertex models) is a neighborhood defined by Voronoi cells (through their Delaunay triangulation) [20,42,80,81]. Such approaches have continuous and physically accurate transitions only if the interactions explicitly depend on the cells' shared surface area. Typically Voronoi neighboring (or similar schemes) will result in more stable cell sheets compared to nearest-neighbor schemes (such as the present) since sheet confluence is easier

to maintain when neighbor interaction weights do not decay with distance. Our model could be adapted to use Voronoi or similar neighbor schemes. However, our differentiable programming approach will be more involved in such cases if we require that our potential remains continuous. Nonetheless, such extensions could make our system more robust against large preferred curvature strains. The fact that the present model's sheets are stable with just using a nearest-neighbor scheme is due to the carefully chosen V_{sheet} term in our potential.

The present model has the potential to model a wide range of shape transformations seen in biology, such as morphogenesis of *Hydra* [82] or the gastrulation of *Drosophila* [83]. For simple morphological transformation, the input of an initial shape and a final shape is enough to define the full morphological process by using simple signaling functions such as the one exemplified here. For more intricate transformations, more complex signaling is needed. In principle, deriving such signaling could also be automated using a neural network or differentiable programming approaches to emulate gene regulatory networks [68]. We have not discussed the analysis of the forces, stretches, and stresses that arise in the morphological transformations the model predicts. This is an interesting perspective, but one that is slightly complicated by the nature of cell rearrangements: while the final shape obtained is robust to perturbations, which cells end up where is not robust to noise. Such analysis thus needs to be global and not depend on specific migratory paths of single cells.

Studies of morphological processes typically impose a set of parameters and then analyze the shapes that emerge. This is the case for both vertex models [35,39] and centroid models [42]. Here we have demonstrated that the opposite approach is also viable and have shown that both shape deformations and neighbor rearrangements can be simultaneously driven by the same potential function.

ACKNOWLEDGMENTS

[1] J. A Ampos-Ortega and V. Hartenstein, *The Embryonic Development of Drosophila Melanogaster* (Springer Science, Berlin, 2013)

[2] E. B. Lewis, A gene complex controlling segmentation in Drosophila, Nature (London) **276**, 565 (1978).

[3] P. A. Lawrence, *The Making of a Fly: The Genetics of Animal Design* (Wiley-Blackwell, Oxford, UK, 1992).

[4] D. St. Johnston, W. Driever, T. Berleth, S. Richstein, and C. Nusslein-Volhard, Multiple steps in the localization of bicoid RNA to the anterior pole of the Drosophila oocyte, Development **107**, 13 (1989).

[5] S. B. Carroll, Zebra patterns in fly embryos: Activation of stripes or repression of interstripes? Cell **60**, 9 (1990).

[6] R. Rivera-Pomar and H. Jäckle, From gradients to stripes in Drosophila embryogenesis: Filling in the gaps, Trends Genet. **12**, 478 (1996).

[7] H. Janssens, S. Hou, J. Jaeger, A. R. Kim, E. Myasnikova, D. Sharp, and J. Reinitz, Quantitative and predictive model of transcriptional control of the Drosophila melanogaster even skipped gene, Nat. Genet. **38**, 1159 (2006).

[8] M. D. Petkova, G. Tkačik, W. Bialek, E. F. Wieschaus, and T. Gregor, Optimal decoding of cellular identities in a genetic network,Cell **176**, 844 (2019).

[9] A. Zubair, I. G. Rosen, S. V. Nuzhdin, and P. Marjoram, Bayesian model selection for the Drosophila gap gene network, BMC Bioinf. **20**, 327 (2019).

[10] E. Farge, Mechanical induction of twist in the Drosophila Foregut/Stomodeal Primordium, Curr. Biol. **13**, 1365 (2003).

[11] E. Hannezo, J. Prost, and J. F. Joanny, Instabilities of Monolayered Epithelia: Shape and Structure of Villi and Crypts, Phys. Rev. Lett. **107**, 078104 (2011).

[12] S. Lin, Y. M. Xie, Q. Li, X. Huang, Z. Zhang, G. Ma, and S. Zhou, Shell buckling: From morphogenesis of soft matter to prospective applications, Bioinspir. Biomim. **13**, 051001 (2018).

[13] T. A. Engstrom, T. Zhang, A. K. Lawton, A. L. Joyner, and J. M. Schwarz, Buckling without Bending: A New Paradigm in Morphogenesis, Phys. Rev. X **8**, 041053 (2018).

[14] J. B. Kirkegaard, B. F. Nielsen, A. Trusina, and K. Sneppen, Self-assembly, buckling, and density-invariant growth of three-dimensional vascular networks, J. R. Soc. Interface, **16**, 20190517 (2019).

[15] D. S. Vijayraghavan and L. A. Davidson, Mechanics of neurulation: From classical to current perspectives on the physical mechanics that shape, fold, and form the neural tube, Birth Defects Res. **109**, 153 (2017).

[16] B. F. Nielsen, S. B. Nissen, K. Sneppen, J. Mathiesen, and A. Trusina, Model to link cell shape and polarity with organogenesis, iScience **23**, 100830 (2020).

[17] X. Chen and G. Wayne Brodland, Multi-scale finite element modeling allows the mechanics of amphibian neurulation to be elucidated, Phys. Biol. **5**015003 (2008).

[18] G. W. Brodland and D. A. Clausi, Embryonic tissue morphogenesis modeled by FEM, J. Biomech. Eng. **116**, 146 (1994).

[19] J. Hardin and R. Keller, The behaviour and function of bottle cells during gastrulation of Xenopus laevis, Development **103**, 211 (1988).

[20] D. Drasdo and G. Forgacs, Modeling the interplay of generic and genetic mechanisms in cleavage, blastulation, and gastrulation, Dev. Dyn. **219**, 182 (2000).

[21] B. Vasiev, A. Balter, M. Chaplain, J. A. Glazier, and C. J. Weijer, Modeling gastrulation in the chick embryo: Formation of the primitive streak, PLoS ONE **5**, e10571 (2010).

[22] B. Roberto, E. R. Rojas, and J. Dumais, The mechanics of tip growth morphogenesis: what we have learned from rubber balloons, J. Mech. Mater. Struct. **2**, 1157 (2007).

[23] S. Bartnicki-Garcia, F. Hergert, and G. Gierz, Computer simulation of fungal morphogenesis and the mathematical basis for hyphal (tip) growth, Protoplasma **153**, 46 (1989).

[24] J. Dumais, S. L. Shaw, C. R. Steele, S. R. Long, and P. M. Ray, An anisotropic-viscoplastic model of plant cell morphogenesis by tip growth, Int. J. Dev. Biol. **50**, 209 (2006).

[25] S. Höhn, A. R. Honerkamp-Smith, P. A. Haas, P. K. Trong, and R. E. Goldstein, Dynamics of a *Volvox* Embryo Turning Itself Inside Out, Phys. Rev. Lett. **114**, 178101 (2015).

[26] P. A. Haas and R. E. Goldstein, Elasticity and glocality: Initiation of embryonic inversion in Volvox, J. R. Soc. Interface. **12**, 20150671 (2015).

[27] P. A. Haas, S. S. M. H. Höhn, A. R. Honerkamp-Smith, J. B. Kirkegaard, and R. E. Goldstein, The noisy basis of morphogenesis: Mechanisms and mechanics of cell sheet folding inferred from developmental variability, PLoS Biol. **16**, e2005536 (2018).

[28] J. Sharpe, Computer modeling in developmental biology: Growing today, essential tomorrow, Development **144**, 4214 (2017).

[29] J. A. Izaguirre, R. Chaturvedi, C. Huang, T. Cickovski, J. Coffland, G. Thomas, G. Forgacs, M. Alber, G. Hentschel, S. A. Newman, and J. A. Glazier, CompuCell, a multi-model framework for simulation of morphogenesis, Bioinformatics **20**, 1129 (2004).

[30] R. Merks, A. Hoekstra, J. Kaandorp, and P. Sloot, Models of coral growth: Spontaneous branching, compactification and the Laplacian growth assumption, J. Theor. Biol. **224**, 153 (2003).

[31] R. M. A. Vroomans, P. Hogeweg, and K. H. W. J. ten Tusscher, Segment-Specific Adhesion as a Driver of Convergent Extension, PLoS Comput. Biol. **11**, e1004092 (2015).

[32] S. Alt, P. Ganguly, and G. Salbreux, Vertex models: From cell mechanics to tissue morphogenesis, Philos. Trans. R. Soc. B **372**, 20150520 (2017).

[33] T. Nagai and H. Honda, A dynamic cell model for the formation of epithelial tissues, Philos. Mag. B **81**, 699 (2001).

[34] R. Farhadifar, J.-C. Röper, B. Aigouy, S. Eaton, and F. Jülicher, The influence of cell mechanics, cell-cell interactions, and proliferation on epithelial packing, Curr. Biol. **17**, 2095 (2007).

[35] D. L. Barton, S. Henkes, C. J. Weijer, and R. Sknepnek, Active vertex model for cell-resolution description of epithelial tissue mechanics, PLoS Comput. Biol. **13**, e1005569 (2017).

[36] M. Misra, B. Audoly, I. G. Kevrekidis, and S. Y. Shvartsman, Shape transformations of epithelial shells, Biophys. J. **110**, 1670 (2016).

[37] C. Bielmeier, S. Alt, V. Weichselberger, M. La Fortezza, H. Harz, F. Jülicher, G. Salbreux, and A. K. Classen, Interface contractility between differently fated cells drives cell elimination and cyst formation, Curr. Biol. **26**, 563 (2016).

[38] A. G. Fletcher, M. Osterfield, R. E. Baker, and S. Y. Shvartsman, Vertex models of epithelial morphogenesis, Biophys. J. **106**, 2291 (2014).

[39] J. Rozman, M. Krajnc, and P. Ziherl, Collective cell mechanics of epithelial shells with organoid-like morphologies, Nat. Commun. **11**, 3805 (2020).

[40] G. R. Mirams, C. J. Arthurs, M. O. Bernabeu, R. Bordas, J. Cooper, A. Corrias, Y. Davit, S. J. Dunn, A. G. Fletcher, D. G. Harvey, M. E. Marsh, J. M. Osborne, P. Pathmanathan, J. Pitt-Francis, J. Southern, N. Zemzemi, and D. J. Gavaghan, Chaste:

[41] M. Marin-Riera, M. Brun-Usan, R. Zimm, T. Välikangas, and I. Salazar-Ciudad, Computational modeling of development by epithelia, mesenchyme and their interactions: A unified model, Bioinformatics **32**, 219 (2016).

[42] S. B. Nissen, S. Rønhild, A. Trusina, and K. Sneppen, Theoretical tool bridging cell polarities with development of robust morphologies, eLife **7**, e38407 (2018).

[43] P. Germann, M. Marin-Riera, and J. Sharpe, yalla: GPU-Powered spheroid models for mesenchyme and epithelium, Cell Systems **8**, 261 (2019).

[44] J. Prost, F. Jülicher, and J.-F. Joanny, Active gel physics, Nat. Phys. **11**, 111 (2015).

[45] J. Genzer and J. Groenewold, Soft matter with hard skin: From skin wrinkles to templating and material characterization, Soft Matter **2**, 310 (2006).

[46] B. Li, Y. P. Cao, X. Q. Feng, and H. Gao, Mechanics of morphological instabilities and surface wrinkling in soft materials: A review, Soft Matter **8**, 5728 (2012).

[47] V. Conte, J. J. Muñoz, and M. Miodownik, A 3D finite element model of ventral furrow invagination in the Drosophila melanogaster embryo, J. Mech. Behav. Biomed. Mater. **1**, 188 (2008).

[48] W. Helfrich, Elastic properties of lipid bilayers: Theory and possible experiments, Z. Naturforsch. **28**, 693 (1973).

[49] J. Zimmerberg and M. M. Kozlov, How proteins produce cellular membrane curvature, Nat. Rev. Mol. Cell Biol. **7**, 9 (2006).

[50] S. Knoche and J. Kierfeld, Buckling of spherical capsules, Phys. Rev. E **84**, 046608 (2011).

[51] J. R. Frank and M. Kardar, Defects in nematic membranes can buckle into pseudospheres, Phys. Rev. E **77**, 041705 (2008).

[52] G. M. Odell, G. Oster, P. Alberch, and B. Burnside, The mechanical basis of morphogenesis. I. Epithelial folding and invagination, Dev. Biol. **85**, 446 (1981).

[53] J. Dervaux and M. Ben Amar, Morphogenesis of Growing Soft Tissues, Phys. Rev. Lett. **101**, 068101 (2008).

[54] M. Pezzulla, N. Stoop, X. Jiang, and D. P. Holmes, Curvature-driven morphing of non-Euclidean shells, Proc. R. Soc. A **473**, 20170087 (2017).

[55] N. C. Heer, P. W. Miller, S. Chanet, N. Stoop, J. Dunkel, and A. C. Martin, Actomyosin-based tissue folding requires a multicellular myosin gradient, Development **144**, 1876 (2017).

[56] E. Hannezo, J. Prost, and J. F. Joanny, Theory of epithelial sheet morphology in three dimensions, Proc. Natl. Acad. Sci. USA **111**, 27 (2014).

[57] M. Terasaki, T. Shemesh, N. Kasthuri, R. W. Klemm, R. Schalek, K. J. Hayworth, A. R. Hand, M. Yankova, G. Huber, J. W. Lichtman, T. A. Rapoport, and M. M. Kozlov, XStacked endoplasmic reticulum sheets are connected by helicoidal membrane motifs, Cell **154**, 285 (2013).

[58] H. Morita, S. Grigolon, M. Bock, S. F. G. Krens, G. Salbreux, and C.-P. Heisenberg, The physical basis of coordinated tissue spreading in zebrafish gastrulation, Dev. Cell **40**, 354 (2017).

[59] N. I. Petridou, S. Grigolon, G. Salbreux, E. Hannezo, and C.-P. Heisenberg, Fluidization-mediated tissue spreading by mitotic cell rounding and non-canonical wnt signalling, Nat. Cell Biol. **21**, 169 (2019).

an open source C++ Library for computational physiology and biology, PLoS Comput. Biol. **9**, e1002970(2013).

[60] M. Zajac, G. L. Jones, and J. A. Glazier, Model of Convergent Extension in Animal Morphogenesis, Phys. Rev. Lett. **85**, 2022 (2000).

[61] D. J. Andrew and A. J. Ewald, Morphogenesis of epithelial tubes: Insights into tube formation, elongation, and elaboration, Dev. Biol. **341**, 34 (2010).

[62] M. Tada and C. P. Heisenberg, Convergent extension: Using collective cell migration and cell intercalation to shape embryos, Development **139**, 3897 (2012).

[63] M. L. Martik and D. R. McClay, New insights from a high-resolution look at gastrulation in the sea urchin, Lytechinus variegatus, Mech. Dev. **148**, 3 (2017).

[64] R. J. Tetley and Y. Mao, The same but different: Cell intercalation as a driver of tissue deformation and fluidity, Philos. Trans. R. Soc. B **373**, 20170328 (2018).

[65] A. C. Humphries and M. Mlodzik, From instruction to output: Wnt/PCP signaling in development and cancer, Curr. Opin. Cell Biol. **51**, 110 (2018).

[66] G. Pezzulo and M. Levin, Top-down models in biology: Explanation and control of complex living systems above the molecular level, J. R. Soc. Interface. **13**, 20160555 (2016).

[67] S. Kriegman, D. Blackiston, M. Levin, and J. Bongard, A scalable pipeline for designing reconfigurable organisms, Proc. Natl. Acad. Sci. USA **117**, 1853 (2020).

[68] A. Mordvintsev, E. Randazzo, E. Niklasson, and M. Levin, Growing neural cellular automata, Distill **5**, e23 (2020).

[69] D. P. Kingma and J. L. Ba, Adam: A method for stochastic optimization, arXiv:1412.6980.

[70] J. Roignot, X. Peng, and K. Mostov, Polarity in mammalian epithelial morphogenesis, Cold Spring Harbor Perspect. Biol. **5**, a013789 (2013).

[71] A. Scholich, S. Syga, H. Morales-Navarrete, F. Segovia-Miranda, H. Nonaka, K. Meyer, W. De Back, L. Brusch, Y. Kalaidzidis, M. Zerial, F. Jülicher, and B. M. Friedrich, Quantification of nematic cell polarity in three-dimensional tissues, PLoS Comput. Biol. **16**, e1008412 (2020).

[72] H. McNeill, Planar cell polarity: keeping hairs straight is not so simple. Cold Spring Harbor Perspect. Biol. **2**, a003376 (2010).

[73] C. Duclut, A. Amiri, J. Paijmans, and F. Jülicher, Coarse-grained curvature tensor on polygonal surfaces, SciPost Phys. Core **5**, 011 (2022).

[74] G. H. Golub and V. Pereyra, The differentiation of pseudo-inverses and nonlinear least squares problems whose variables separate, SIAM J. Numer. Anal. **10**, 413 (1973).

[75] A. Paszke, S. Gross, F. Massa, A. Lerer, J. Bradbury, G. Chanan, T. Killeen, Z. Lin, N. Gimelshein, L. Antiga, A. Desmaison, A. Köpf, E. Yang, Z. DeVito, M. Raison, A. Tejani, S. Chilamkurthy, B. Steiner, L. Fang, J. Bai *et al.*, PyTorch: An imperative style, high-performance deep learning library, Adv. Neural Inform. Process. Syst. **32** (2019).

[76] See Supplemental Material at http://link.aps.org/supplemental/10.1103/PhysRevResearch.4.023171 for (1) Video showing the formation of the squidlike shape. (2) Python code implementing the approach and demonstrating morphogenesis of shapes supplied as OBJ files (examples included).

[77] A. M. Turing, The chemical basis of morphogenesis, AIBS Bull. **52**, 55 (1952).

[78] D. Papatsenko and M. Levine, The drosophila gap gene network is composed of two parallel toggle switches, PLoS ONE **6**, e21145 (2011).

[79] D. Bi, J. H. Lopez, J. M. Schwarz, and M. Lisa Manning, Energy barriers and cell migration in densely packed tissues, Soft Matter **10**, 1885 (2014).

[80] G. W. Brodland and J. H. Veldhuis, Computer simulations of mitosis and interdependencies between mitosis orientation, cell shape, and epithelia reshaping, J. Biomech. **35**, 673 (2002).

[81] H. Honda, M. Tanemura, and T. Nagai, A three-dimensional vertex dynamics cell model of space-filling polyhedra simulating cell behavior in a cell aggregate, J. Theor. Biol. **226**, 439 (2004).

[82] Y. Maroudas-Sacks, L. Garion, L. Shani-Zerbib, A. Livshits, E. Braun, and K. Keren, Topological defects in the nematic order of actin fibres as organization centres of hydra morphogenesis, Nat. Phys. **17**, 251 (2021).

[83] M. Leptin, Drosophila gastrulation: From pattern formation to morphogenesis, Annu. Rev. Cell Dev. Biol. **11**, 189 (1995).